International Journal of Heat and Technology
Vol. 42, No. 5, October, 2024, pp. 1660-1670
Journal homepage: http://iieta.org/journals/ijht

Numerical Study of a Wickless Heat Pipe for Cooling of Electronic Component

Samah Ehsan Adnan[1], Muna S. Kassim[1], Nabeh Alderoubi[2], Hakim S. Sultan Aljibori[3], Saif Yousif Ibrahim[1], Raid Ahmed Mahmood[4], Hasan Shakir Majdi[5], Laith Jaafer Habeeb[6*]

[1] Mechanical Engineering Department, College of Engineering, Mustansiriyah University, Baghdad 10052, Iraq
[2] Design and Drafting Technology Department, Lincoln Campus, Southeast Community College, Nebraska Lincoln 68521, USA
[3] College of Engineering, University of Warith Al-Anbiyaa, Karbala 56001, Iraq
[4] School of Engineering, University of Southern Queensland, Toowoomba 4350, Australia
[5] Department of Chemical Engineering and Petroleum Industries, Al-Mustaqbal University College, Hillah 51001, Iraq
[6] Training and Workshop Center, University of Technology- Iraq, Baghdad 10066, Iraq

Corresponding Author Email: Laith.J.Habeeb@uotechnology.edu.iq

https://doi.org/10.18280/ijht.420520

Received: 18 April 2024
Revised: 20 July 2024
Accepted: 5 August 2024
Available online: 31 October 2024

Keywords:
wickless heat pipe, fill ratio, saturation temperature, input power

ABSTRACT

This work conducts a numerical analysis on a wickless heat pipe with a flat evaporator (100 mm × 100 mm × 30 mm) designed to cool electronic components. A flat square electrical element of 100 mm × 100 mm is used to generate heat. The objective is to examine the relationship between the thermal performance of wickless heat pipe, its fill ratio, and the flow rate of cooling water. Performance was validated using Engineering Equation Solver (EES) software. Various fill ratios (15%, 25%, 50%, and 85%) and input powers (10 W to 100 W) were considered, with flow rates of cooling water ranging 0.0083 kg/s - 0.033 kg/s. The results indicate that at 100 W input power and a 15% fill ratio, the evaporator wall temperature reached 100°C. The minimum evaporator resistance of 0.07°C/W and condenser resistance of 0.14°C/W were observed at a 50% fill ratio under similar conditions. The optimal cooling water flow rate for this system was found to be 0.016 kg/s.

1. INTRODUCTION

The function of heat pipes is to reroute heat from a source to a heat sink through the evaporation and condensation of a working fluid in an enclosed tube. They are applied in heat exchanges, cooling of electronic parts, and solar systems commonly used to harness energy from the sun due to their low resistance, compact design, and minimal working fluid requirement [1].

Figure 1 is a diagram of a Wickless heat pipe that primarily illustrates these 3 parts; condenser section, evaporator section, and adiabatic section [2]. The same working fluid in the evaporator removes heat from the air, which is consequently rejected in the condenser. The water jacket brings about condensation of the vapor in the condenser section, and the condensate then falls down into the evaporator due to gravity or capillary force, which is the type of heat pipe being used [3].

Simple as the gravitational straight heat pipe is, it is not without its drawbacks, and the most significant one is entrainment, where the heat transfer capacity is affected and there are also increased flow resistances between the liquid and vapor.

In this paper, the thermal characteristics of heat pipes without wick structure for cooling electronics parts are studied with an emphasis on the impact of the fill ratios and cooling water flow rates. This paper starts by presenting a theoretical analysis of wickless heat pipe technology and how the device functions. The next sections describe practical implementations and display different arrangements to achieve the best cooling performance; findings of experimental and numerical analyses are presented here. Last but not the least, the article presents some of the issues and limitations that may be faced during the real-life implementation, and gives ideas for future works in the field, as well as possible improvement in the wickless heat pipe for next generation cooling technology.

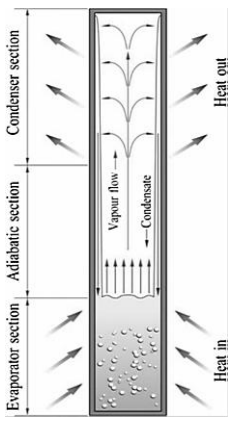

Figure 1. Diagram of wickless heat pipe [2]

2. LITERATURE REVIEW

Several previous studies have investigated different aspects of heat pipes:

Al Jubori and Jawad [4] analyzed numerically, using CFD with ANSYS-Fluent, the temperature distribution and thermal resistance of wickless heat pipe depending on working conditions.

For analyzing thermal performance of oscillating heat pipe (OHP), there is a work done by Barrak et al. [5] who has done experimental and numerical CFD simulation. They utilized water and 50% fill ratio (FR) as the total volume. As for the results, the maximum of the thermal resistance was 1.036 C°/W at 13.75 W.

In having a look at the heat transfer characteristics of a THP's evaporator portion, Kim et al. [6] studied the impact of sintered microporous skin layer at the external surface. A 25 mm internal diameter copper tube of 935 mm length with water as the working fluid was used. The reduction of Rth values was found to be 51% and 30% at the FR of 35% and 70% respectively.

Wang et al. [7] constructed an experimental test rig and used the ANSYS/Fluent software to numerically set up a 2D CFD simulation to study and illustrate the geyser boiling on the inside of a glass thermosyphon heat pipe. The results of the temperature distribution experiment and 2D CFD simulation were in good agreement. The geyser boiling cannot be seen by a high-speed camera, but it can be clearly seen in a 2D CFD simulation.

Eidan et al. [8] presented this aspect experimentally and numerically through FORTRAN code in case of Thermosyphon Heat Pipe (THP). The authors stated that water provides the better TP concerning the other systems in the temperature range of 30℃ to 50℃.

Alammar et al. [9] analyzed the effect of the inclination angle and fill ratio (FR) on the thermal performance of THP employing Ansys R15/Fluent. They discovered that the optimum value of FR is 65%, and thermal efficiency is reduced when THP is closer to the horizontal orientation. The comparison of the 2D CFD solution with the experimental data revealed that the former was approximately. Thus, for the errors of the present model, the calculated THD of the fundamental current is found to be 8.1% higher than the experimental data. It has been planned that the improvement of the temperature distribution of the stator bar and thermal resistance of copper strands would be 1%.

Fadhl et al. [10] used a CFD simulation to study the two-phase closed thermosyphon numerically. Working fluids were R134a and R404a. They discovered that, in comparison to water, the thermal properties of the two fluids in the thermosyphon differ significantly.

Abdullahi [11] studied experimentally and numerically the impacts of input energy and flow rate of cooling on the thermal performance of the thermosyphon heat pipe. In its numerical work, it applies CFD analysis. The finding depicted that the dual-phase closed thermosyphon's heat transfer properties improved with increasing inclination angle and input power.

Anjankar and Yarasu [12] studied effect of condenser length on thermosyphon thermal performance; an experimental investigation was undertaken. They learned that the thermosyphon gives the maximum result when flow is 0.0027 kg/sec, and power is 500 W.

Jiao et al. [13] studied that a vertical two-phase closed thermosyphon's steady-state heat transfer performance was affected by fill ratio (TPCT). In their experimental work, they used nitrogen as the working fluid and two different TPCT geometries. Based on their investigation and comparison, they concluded that the fill ratio range needed to keep a TPCT stable and productive is present.

Wang et al. [14] examined the impact of non-homogeneous heat input rates on a vertical two-phase closed thermosyphon (TPCT). An evaporation and condensation model based on the computational fluid dynamics (CFD) method was applied to the TPCT. Alkhafaj et al. [15] are examining the working conditions of the wickless heat pipe with R1234-yf and ethanol as the working fluids at different temperatures and different filling ratios. Consequently, the results indicated that the pipe had the best thermal performance of 0.181 with a filling ratio of 60%. The working fluid used in this study was ethanol. A new approach was used to forecast the total thermal performance.

Despite the extensive research, there is still a need to analyze the thermal performance of wickless heat pipes under varying fill ratios and cooling water flow rates, especially for electronic cooling applications. This work intends to achieve this by carrying out a numerical analysis using EES software to fill the existing gap.

3. THEATRICAL ANALYSIS

The analysis can be classified as the heat pipe the straight one. Two features characterize the type considered; the first is the relatively small dimensions of its components. The second feature is the low working fluid velocity, which is a characteristic feature in all thermosyphon systems. Accordingly, frictional losses are ignored in the analysis. The theoretical modeling will focus on thermal analysis of the evaporator and condenser. Figure 2 shows the diagram of straight heat pipe. Vapor and the condensate continue their motion in a straight pipe. Vapor usually moves upward while the condensate always descends due to gravity.

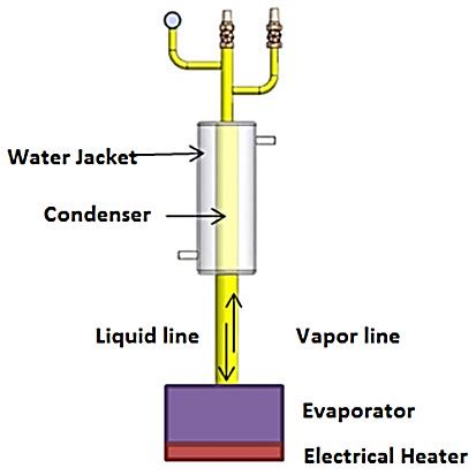

Figure 2. Diagram of straight heat pipe under consideration

The theoretical model assumptions are:

1. Mass flow rate and heat transfer rate are constant.
2. Because of the short straight pipe lengths, the low mass flow rate, and the gravitational pressure gradient, frictional pressure losses in the pipes are disregarded [16].

3. In the studied the system is transfer heat by natural convection to ambient air. All components of the devices are supposed to well insulate and the thermal losses from these parts are neglected.

4. Thermophysical properties of fluid change with temperature.

5. Inlet temperature of cooling water is constant.

The superficial forces between the rising vapor and falling liquid in a straight heat pipe are neglected [17].

4. THEORETICAL MODEL

A steady state, one-dimensional, two-phase flow model is developed to predict the operation condition of system based on mass, momentum, and energy conservation.

4.1 Conservation of mass (continuity equation)

The continuity equation is implicitly satisfied by assuming a constant value of the mass flow rate throughout the straight heat pipe. This requires that the rate of evaporation in the evaporator equal the rate of condensation in the condenser.

$$\dot{m} = \dot{m}_{evap} = \dot{m}_{cond} \tag{1}$$

4.2 Conservation of momentum

Two terms in the momentum equation affect the performance of single-phase and two-phase thermosyphon, namely, the frictional term and the gravitational term. In a two-phase loop considered in the present work, the frictional effects may be neglected in comparison with the gravitation term. This assumption is justified by two facts: the first is the short distance traveled by the working fluid, and the second fact is the low value of mass flow rate, which hardly produces noticeable frictional losses [17].

Head pressure = Friction losses:

$$\Delta p = \rho \, g \, H \tag{2}$$

4.3 Conservation of energy

The energy equation is satisfied in the straight by assuming that any heat received in the evaporator is delivered in the condenser. This is, of course, applied by neglecting any thermal losses to the environment. To apply the energy equation, thermal models are used in the evaporator and the condenser to estimate the heat absorbed and rejected, respectively.

4.4 Thermal analysis of the evaporator

The evaporator in the present work takes the form of a small container that receives heat from its bottom side. The condensate returned from the condenser enters the evaporator in an assumed subcooled condition. It must be heated to the boiling point corresponding to the existing pressure in order to evaporate. The generated vapor may also be superheated in the part of the evaporator that is not filled with liquid. To simplify the analysis, the evaporator geometry is simplified theoretically to a straight tube at which the working fluid undergoes the three states of subcooling, boiling, and superheating as it flows through it, as can be seen in Figure 3.

In this figure, the areas A, A, and A represent the three zones at which subcooling, boiling, and superheating take place within the evaporator section.

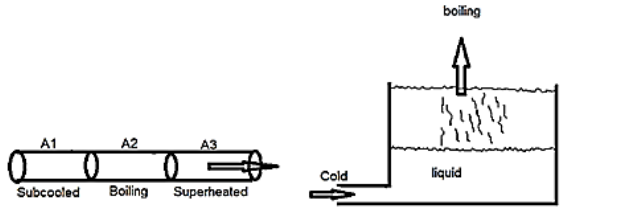

Fig (a) Hypothetical evaporator **Fig (b) actual evaporator**

Figure 3. Simplification of the geometry of evaporator

Before the study of the thermal performance of the three states, three main parameters should be calculated: Mass flow rate, wall evaporator temperature, and saturation temperature. The parameters are common for the three regions. There is also a fourth parameter, which is the heat transfer coefficient. This coefficient is calculated separately for each of the three regions but using a unified procedure. These parameters are discussed first before detailing the thermal calculations for each evaporator region [18].

4.4.1 Subcooled region

The main inflow with the working fluid goes to the evaporator already at the subcooled condition that is at T_1 temperature level. If the saturation temperature *Tsat* is identified at that, the wall temperature T_w, which too characterizes the area of the subcooled section, is estimated by the next equation modified from [19]:

$$A_1 = \dot{m} \, cp_l \, \frac{(Tsat - T_1)}{h_1 \left(T_w - T_{avg1}\right)} \tag{3}$$

$$T_{avg1} = \frac{Tsat + T_1}{2} \tag{4}$$

where, Q_1 is the suitable heat advance of the subcooled region can be calculated by the subsequent equation:

$$Q_1 = \dot{m} \, cp_l (Tsat - T_1) \tag{5}$$

The parameters, T_w, *Tsat*, T_1, ṁ, h_1 in the above equations are not known in advance. h_1 is connective heat transfer coefficient of the liquid working fluid in the subcooled region of the evaporator.

The value of h_1 depends on the type of the flow inside the tubes whether it is laminar, turbulent or transitional. A check on the flow type need, so be done to determine which heat transfer equation is to be used.

The present work by the calculation of the flow Reynolds Number (Re) inside the heat pipes.

If Re is below 2000, the flow is considered laminar. If it is over 2300, the flow is considered turbulent, and if Re lies between 2000 and 2300, the flow is considered transitional [20]. In the study, the flow type is considered laminar because, in the present work, small dimensions and low velocities are used.

For laminar flow with constant heat flux, the liquid heat transfer coefficient (htc) is estimated by the following equation:

$$\frac{h_1 D}{k_l} = 4.36 \quad (6)$$

4.4.2 Boiling region

The useful heat addition in the boiling section, which is a purpose of A_2, is determined by the following equation [21]:

$$Q_2 = h_2 A_2 [T_W - Tsat] \quad (7)$$

A_2 is the boiling region area. The following equation is then used to compute the rate of boiling that equals the mass flow rate of the working fluid:

$$\dot{m} = \frac{Q_2}{h_{fg}} \quad (8)$$

h_2: boiling heat transfer and (htc): coefficient proposed by Reshenow [22].

$$h_2 = \frac{q_2}{(T_w - Tsat)} \quad (9)$$

$$q_2 = \mu_l h_{fg} \left[\frac{9.81(\rho_l - \rho_v)}{\sigma}\right]^{0.5} \left[\frac{cp_l (Tw - Ts)}{0.01 h_{fg} \left(\left(\frac{\mu_l cp_l}{k_l}\right)^{1.7}\right)}\right]^{1.8} \quad (10)$$

The evaporator resistance R_{evap} is inverse of the evaporation heat transfer coefficient and surface area of the evaporator. The evaporator resistance considered by the following equation:

$$R_{evap} = \frac{1}{h_2 A} \quad (11)$$

4.4.3. Superheated region

The following equation is then used to compute the rate of boiling:

$$T_2 = Tsat + \frac{Q_3}{\dot{m}\, cp_v} \quad (12)$$

The following equation estimates Q_3, which is the beneficial heat gain for superheated region:

$$Q_3 = h_3 A_3 (T_W - T_{avg2}) \quad (13)$$

$$T_{avg2} = \frac{T_{sat} + T_2}{2} \quad (14)$$

$$A_3 = \frac{\dot{m}\, cp_v (T_2 - Tsat)}{h_3 (T_w - T_{avg2})} \quad (15)$$

The vapor working fluid's connective heat transfer coefficient in the superheated area is h_3. It is computed using the same equations as for the liquid phase, but with the vapor phase's attributes in place of the liquid phase's.

4.5 Upriser

The upriser is supposed to be well isolated; therefore, the thermal losses from the upriser are neglected. The working fluid condition at the evaporator outlet will therefore be considered as the input condition to the condenser.

4.6 Thermal analysis of the condenser

The condenser incorporates the same methodology used to analyze the two-phase evaporator. Two regions of the condenser will be divided. Superheated vapor enters the condenser in the first region, close to the condenser inlet, where it will be desuperheated to saturation temperature. Whenever the temperature is lower than the vapor saturation temperature, condensation will start at the condenser's interior walls simultaneously. If the system's fill ratio is high enough, liquid fluid will overflow the condenser's lower part. This flooded region of the condenser contains the subcooled area. The second section of the condenser analysis is the section at which the subcooling process begins. As a result, the system filling ratio will determine whether there is a subcooled region in the condenser section.

4.6.1 Condensation region

In the first condensation region, the first region area is estimated by the following equation:

$$A_4 = \frac{\dot{m} cpv (T_2 - Tsat)}{h_4 (T_{avg2} - T_{cw})} \quad (16)$$

T_{cw} is the average water cooling temperature is considered by the following equation:

$$T_{cw} = \frac{T_{w1} + T_{w2}}{2} \quad (17)$$

h_4 is the connective heat transfer coefficient of the vapor at the condenser inlet.

The following equation determines heat rejection to water jacket in the condensation zone in the second region:

$$Q_5 = h_5 A_5 (Tsat - T_{cw}) \quad (18)$$

where, h_5 is the conventional condensation heat transfer (htc) coefficient which is considered by used equation [23]:

$$h_5 = 0.943 \left[\frac{9.81 \rho_l (\rho_l - \rho_v) h_{fg}\, k_l{}^3}{cp_v \mu_l (Tsat - T_{cw})}\right]^{0.25} \quad (19)$$

The condenser resistance is inverse of the condensation heat transfer coefficient (htc) and surface area of the condenser. The condenser resistance is calculated by the next equation:

$$R_{cond} = \frac{1}{h_5 A} \quad (20)$$

The total resistance can be calculated using summation of the evaporator resistance and condenser resistance [24].

$$R_{total} = R_{boil} + R_{cond} \quad (21)$$

The following equation determines the condensation flow rate, which is equal to the working fluid mass flow rate ($\dot{m}$):

$$\dot{m} = \frac{Q_5}{h_{fg}} \quad (22)$$

4.6.2 Subcooled region

The working fluid will experience subcooling here as the space for condensation decreases as the condenser fills with liquid. The following calculation determines the total interior area of the condenser pipes for subcooling:

$$A_6 = \dot{m} cp_l \frac{(Tsat - T_1)}{h_6 (T_{avg1} - T_{cw})} \quad (23)$$

h_6 is liquid heat transfer coefficient at the condenser determined by the same equation of the liquid heat transfer coefficient at the evaporator.

The heat rejection (Q_6) t:

$$Q_6 = \dot{m} cp_l (Tsat - T_1) \quad (24)$$

The useful heat gain:

$$Q_w = \dot{m}_w cp_w (T_{w2} - T_{w1}) \quad (25)$$

T_{w1}, T_{w2} are the inlet and outlet temperature of the water cooling.

The overall heat input from heater is sum of the useful heat gain by the evaporator or the condenser.

$$Q_{heater} = Q_1 + Q_2 + Q_3 \quad (26)$$

or

$$Q_{heater} = Q_4 + Q_5 + Q_6 \quad (27)$$

4.7 Downcomer

The downcomer is supposed to be well isolated, and its thermal losses to the ambient are neglected. Therefore, the working fluid temperature at the condenser exit will be considered as the temperature at the evaporator inlet.

4.8 Solution procedure

The Engineering Equation Solver program (EES) solves the equations from (1) to (27). This program solves any system of nonlinear ordinary equations. The program also has the facility of automatically providing the thermophysical properties of the working fluid at any location in the solved equations and as a function of the temperature.

The 27 equations mentioned earlier in the part are fed to the program along with the required initial values. The number of the unknowns should equal the number of equations. The constant values constituting the input data to the program are:

1. Basic system dimensions are length of evaporator, length of condenser, area of evaporator and condenser, and diameter of pipe.
2. Temperature of cooling water.
3. Flow rate cooling water.
4. Overall input power.

The idea of interest in this case is a thermal consideration of heat exchangers with reference to phase change in evaporator and condenser parts including subcooled boiling and superheated sections.

Subcooled Region: This is the state at which the fluid is cooler than the saturation temperature. Heat is conducted to the fluid, thereby raising the temperature of the fluid to that of saturation temperature without boiling.

Boiling Region: In this area, the fluid is at its saturation temperature and goes through a phase change from liquid to vapor. Heat used in the change of phase of a substance is referred to as latent heat while it is added during this process.

Superheated Region: After boiling, any addition of heat will add to the temperature of the vapor beyond the saturation temperature.

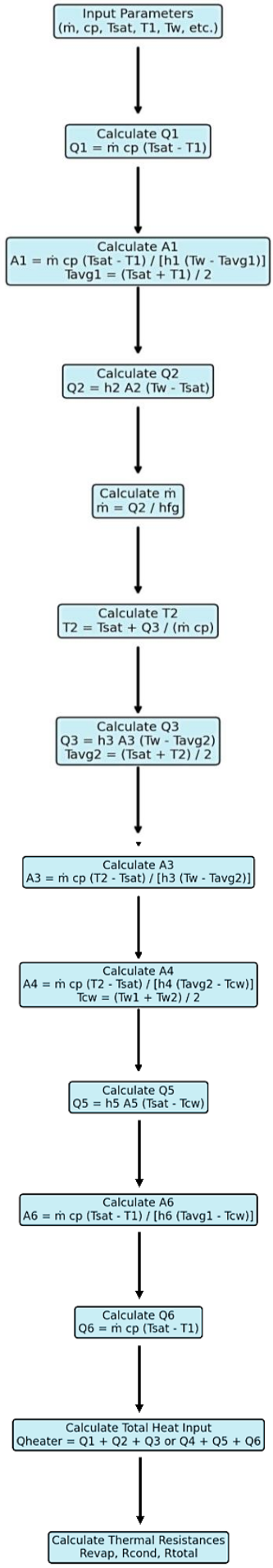

Figure 4. Computation flowchart

Condenser: This is the place where the vapor gives out its heat of condensation and again turns into liquid. The heat rejection process entails the condensation stage and the subcooling stage.

The heat exchanger system model is theoretical, and the stages in the heat exchanging system include subcooled, boiling, superheated, and condensation zones. Certain heat transfer relations and the properties of fluid characterize every stage. The flowchart provides the procedure of calculating for the theoretical model of the heat exchanger system. It presents the flow of analyses and the computations that are required for arriving at the rates of heat transfer, the surface areas, temperatures, and thermal resistances for various areas. Therefore, it is clear that Figure 4 outlines the flow of the thermal analysis.

5. RESULTS AND DISCUSSION

In order to get a theoretical estimation of the thermal performance of heat pipe systems, the commercial software Engineering Equation Solver (EES) solves equations governing the systems. The software is capable of solving systems of nonlinear sets of equations.

5.1 Evaporator and wall temperature T_w

Figure 5 shows variation between evaporator wall temperature and input power for four fill ratios. The figure shows that for all fill ratios, the wall temperature rises with input power. An evaporator's wall temperature reaches its ideal level at a fill ratio of 15%. Figure 6 illustrates how, for four fill ratios, the evaporator exit temperature varies with input power. The graph demonstrates that the highest evaporator exit temperature for a fill ratio of 15% was 97°C, which corresponds to an input power of 100 W.

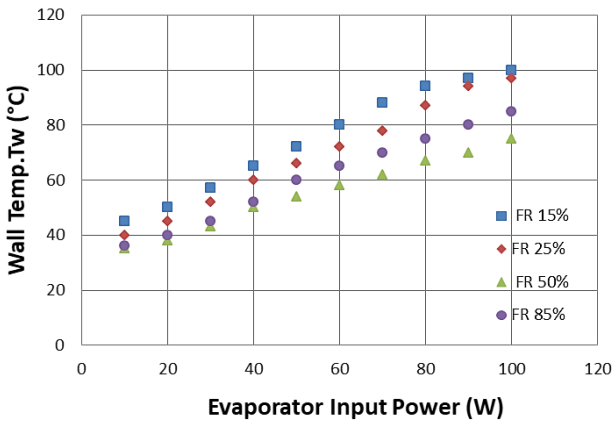

Figure 5. Variation of theoretical wall evaporator temperature

1 Effect of fill ratio

Fill ratio (FR) has a direct influence of the thermal characteristics of the evaporator. The data given depict the antecedent theoretical wall evaporator temperature with respect to the evaporator input power for 15%, 25%, 50%, and 85% fill ratios as shown in figures above.

a) Temperature Trends

i. FR 15%: Thus, when the FR is low, for example, 15%, the rate of increase in temperature with power is slower. This trend indicates that at low power levels, heat dissipation is efficient because there is a smaller volume of liquid, and hence, the liquid is in equilibrium at this stage.

ii. FR 25% and 50%: The fill ratios here depict a moderate temperature rise with power, which is ideal for heat exchange since the liquid-vapor mixture is kept optimal without much heat build-up.

iii. FR 85%: The highest fill ratio shows that the rate of temperature rise is higher at the higher power levels. This could be due to the larger liquid volume, which in order to vaporize takes more energy hence leading to higher wall temperatures.

b) Mechanisms

i. Liquid-Vapor Distribution: Lower fill ratios also mean that there is a higher vapor fraction therefore improving heat transfer by vaporization. On the other hand, the level of fill ratios raises the liquid fraction that in turn can capture more heat but it can be detrimental to heat exchange if not vaporized properly.

ii. Heat Transfer Efficiency: Fill ratios- usually they range from 25% to 50% for liquids, help maintain the right proportion between the liquid and gas phase that is required for efficient heat transfer and thermal stability. At the higher fill ratios (e.g., 85%), the extra liquid may create another layer which may slow down heat transfer.

c) Optimal Fill Ratios

Thus, based on the results presented above, it can be stated that fill ratios within the range of 25-50% are optimal for the best thermal performance of the system. They also keep a constant liquid-vapor interface, which is beneficial to heat transfer and temperature control at the walls. The specific optimum may also depend on the design of the system and operation conditions.

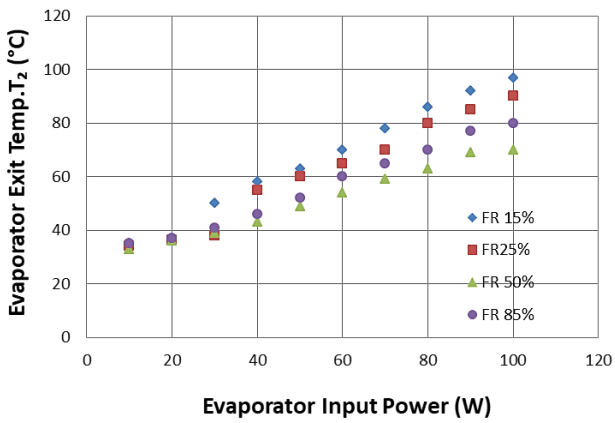

Figure 6. Variation of theoretical evaporator exit temperature with evaporator input power

2 Impact of flow rate

Cooling water flow is very essential in ensuring the intended thermal characteristics. As for the cooling water flow, despite the provided data not giving a direct indication of it, one can analyze its implications based on principles and findings of similar researches.

a) Cooling Efficiency

Raising the flow rate of the cooling water improves the heat dissipation from the system, thus reducing the wall temperatures and improving the thermal characteristics. A high flow rate is important to guarantee that the heat exchanging surfaces are efficient in taking heat away from the

evaporator.

b) Flow Rate Data Analysis

The research done has indicated that the right flow rates of cooling water lead to lower temperatures. For example, a flow rate that conforms to the heat load implies that heat is effectively removed without using a lot of energy. That is why the flow rate cannot be too high, since it only leads to negative results and additional costs.

c) Practical Considerations

i. Energy Consumption: Closely related to this is the management of the cooling rate which serves to control the rate at which the flow is managed to ensure that a balance between cooling and the energy being used is achieved. The design of systems should be such that they can work within the flow rate that is most efficient in removing heat without using too much energy.

ii. System Design Constraints: Other parameters for example, pump capacity, pipe diameter, and heat exchanger affect the achievable flow rate. Proper sizing and maintenance of the system components is therefore a vital factor to be put into consideration.

To enrich the result section with rich result expression, the possibility is to include temperature cloud maps, tabular data, and other graphic images to illustrate the temperature distribution and changes.

Here below is an example of a temperature cloud map for the evaporator with the fill ratio of 50% and with the input power of 50 W: Figure 7 shows the temperature of the evaporator surface and the color gradient shows surface temperature.

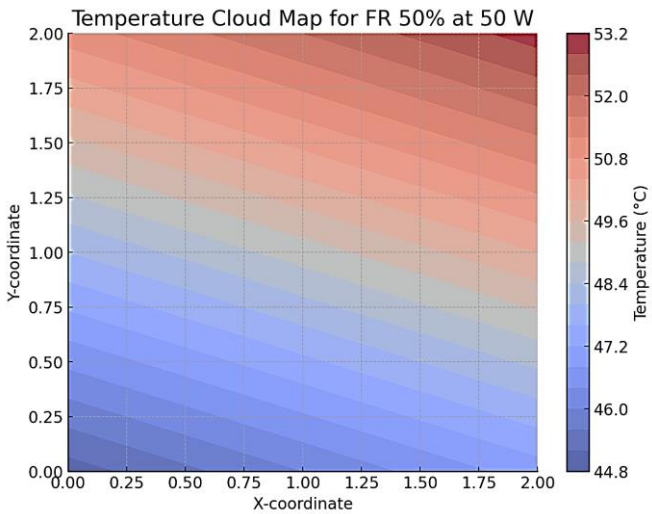

Figure 7. Temperature of the evaporator surface and the color gradient

5.2 Saturation temperature

Straightforwardly, the heat's saturation temperature tends to rise along with the input power in Figure 8, which stands for the change of saturation temperature with input power for four fill ratios. Tests have shown that the saturation temperature reaches its highest value at the fill factor of 85%. Production of any vapor that increases the boiling rate and creates equilibrium between the temperature difference of the fluid and the wall will happen as soon as it occurs. When reading from steam tables, the number that corresponds to the measured saturation pressure is used to estimate the saturation temperature in an indirect manner. Figure 9 illustrates how, for four fill ratios, the predicted evaporator intake temperature varies with evaporator input power. Observed minimum temperatures for 50% fill ratio.

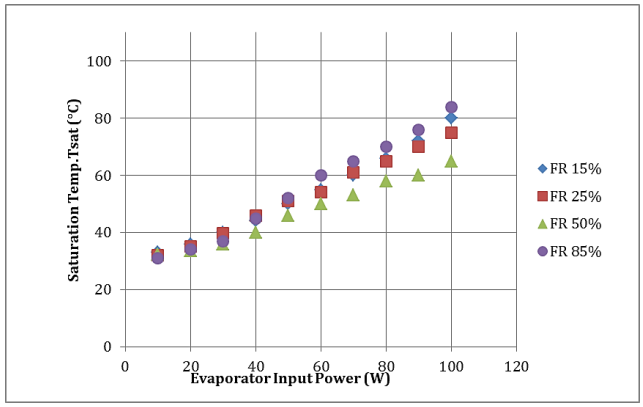

Figure 8. Variation of theoretical saturation temperature

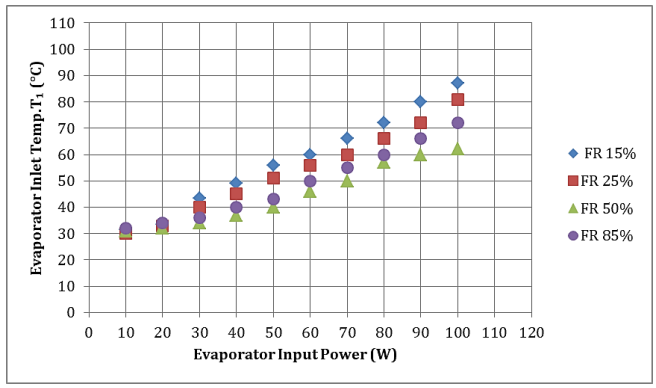

Figure 9. Variation of theoretical evaporator inlet temperature

The following Figure 10 is the temperature cloud map for the fill ratio of 50% based on the upper data. This map graphically shows how the temperature varies with the evaporator input power and the related temperature. The color gradient represents the temperature levels; thus, brighter colors correspond to higher temperatures. From the map, the author presents the temperature rise with the increase in the evaporator input power for the FR of 50%.

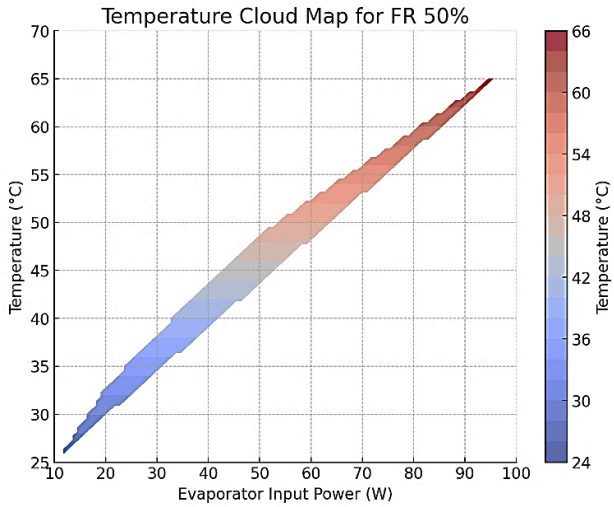

Figure 10. Temperature cloud map for the FR of 50%

5.3 Evaporator heat transfer coefficient

If the saturation and wall temperatures are measured, an approximation of the heat transfer coefficient (h) inside the evaporator can be made. The heat transfer coefficient computed in this manner is a mixture of two processes, namely heat transfer across a single phase and a boiling phase, because the condensate must be heated up to the boiling point before it begins vaporizing. Figure 11 outlines a straightforward relationship between the evaporator h and the level of input power. The evaporation h highest value is 810 W/m^2.°C, which corresponds to an input power of 100 W and a FR of 50%.

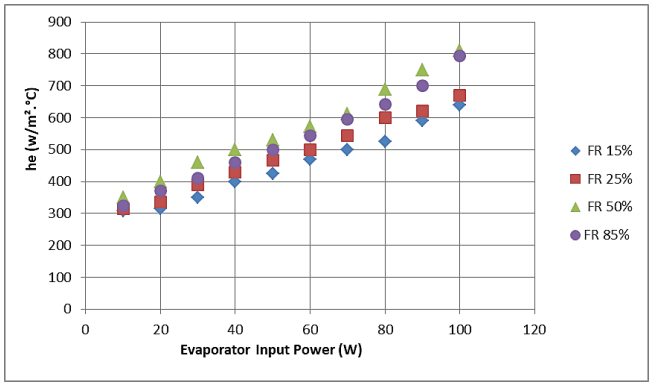

Figure 11. Theoretical evaporation heat transfer coefficient changes its value as evaporator power changes at certain fill ratios

5.4 Thermal resistances

Figures 12 and 13 show the variation of evaporator and condenser resistances as changed with evaporator input power for the four FR. Figures show that for all fill ratios, both condenser and evaporator resistances decrease as input power increases. The figures show that the smallest value of evaporator and condenser resistances occurs at a FR of 50%. Figure 14 shows the difference of the total resistance.

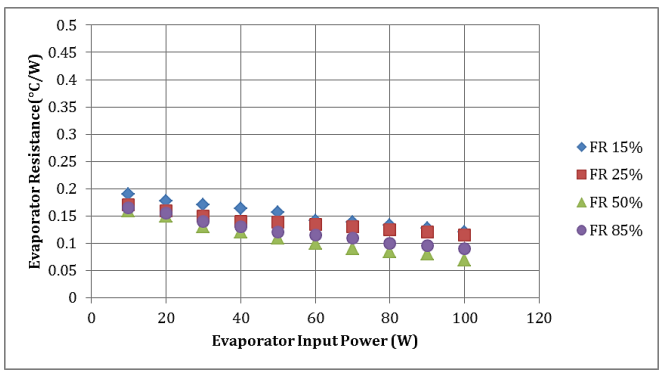

Figure 12. Differential of evaporator resistance linked with evaporator input power for four filling fractions

The following Figure 15 is the condenser resistance cloud map of the fill ratio of 50% estimated from the upper data. This map shows the condenser resistance in relation to the evaporator input power in the specified range. The colors range from low resistance to high resistance and the warmer the color, the higher the resistance. It is possible to observe on the map that the condenser resistance reduces with the growth of the evaporator input power while the fill ratio is 50%.

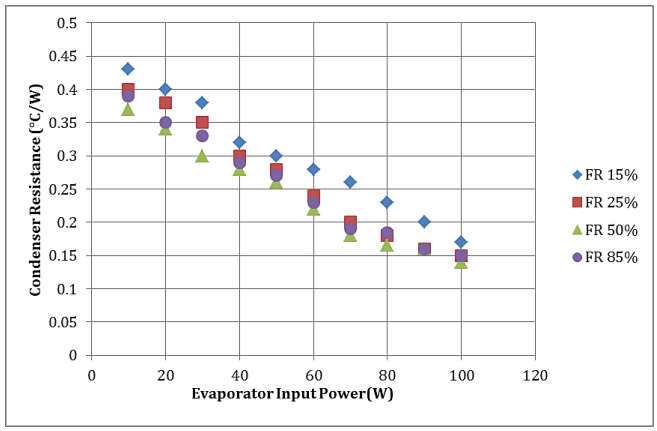

Figure 13. Theoretical condenser resistance

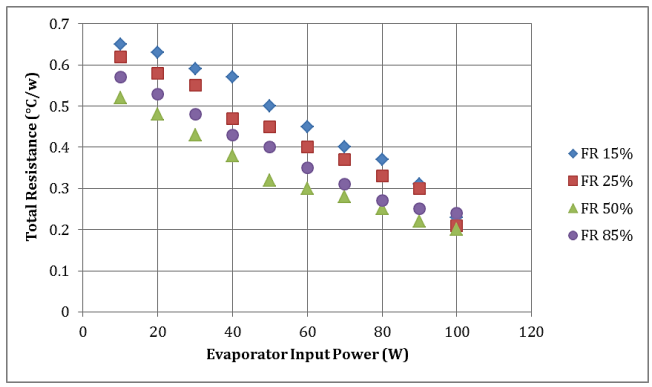

Figure 14. Variation of total resistance

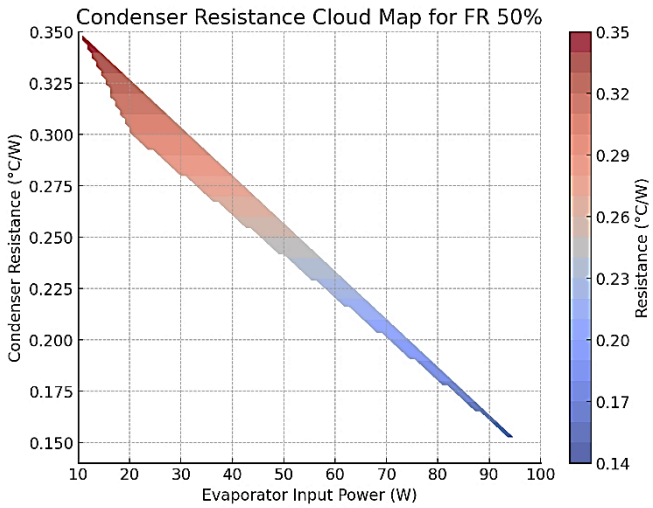

Figure 15. The condenser resistance cloud map of the fill ratio of 50%

5.5 Working fluid

Figure 16 depicts change of the theoretical value of the flow rate of the working fluid with input power of the evaporator, taking into consideration the utilized fill ratios. This is possibly demonstrated more in the figure that shows the working fluid mass flow rate increases steadily with input power for all the FR. Rising fill ratio tends to raise the working fluid mass flow rate due to improvement in the rate of evaporation. An increase in the fill ratios leads to a larger amount of working fluid in the evaporator. This trend is true until a certain limit: the results obtained when using the

appraisals technique cannot be higher than 100 percent. The maximum value of working fluid mass flow rate is 0.00287 kg/s. Similar to the previous case at the input power of 100 W at a FR of 50%.

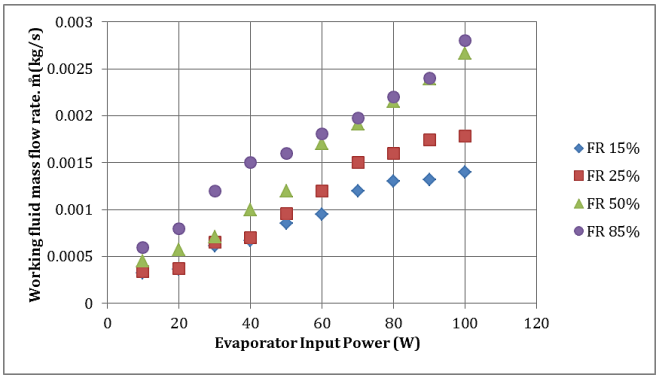

Figure 16. Variation of theoretical working fluid mass flow rate

Figure 17 shows the variation of theoretical value of pressure as changed with working fluid mass flow rate for four fill ratios. Figure 18 shows how, for four fill ratios, the theoretical total resistance varies with flow rate of cooling water at an input power of 50 W. The figure shows that the total resistance reduces as the flow rate of the water increases, and that it then begins to increase at a flow rate of 0.025 kg/s. At flow rate of 0.016 kg/s for cooling water, the total resistance reaches its maximum value.

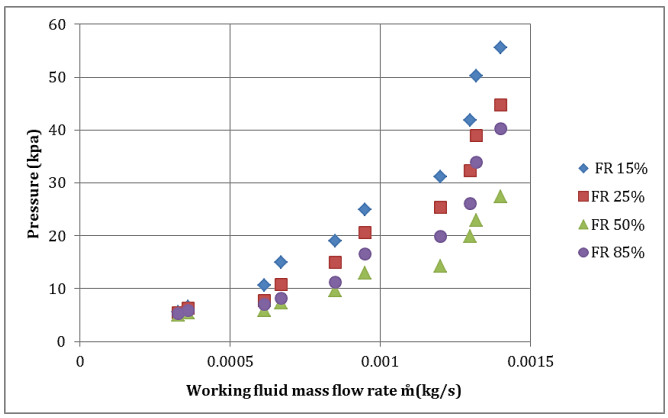

Figure 17. Variation of theoretical pressure

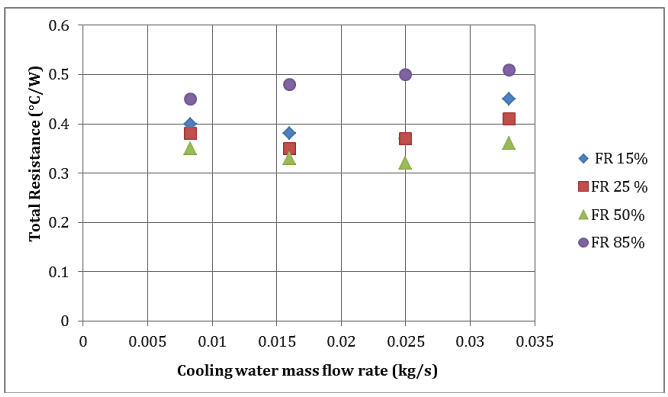

Figure 18. Difference of theoretical total resistance

Figure 19 is the condenser resistance cloud map of the fill ratios of 15%, 25%, 50%, and 85%. The fill ratios have individual colors and small overlapping areas that show the areas of the resistance values.

It is also seen from the map that for each FR the condenser resistance reduces as the evaporator input power increases. This visualization is helpful in comparing the condenser resistance at the various fill ratios for the different power levels.

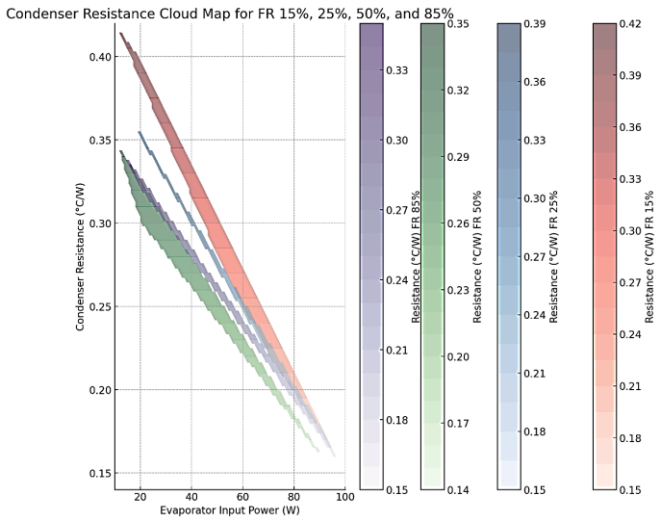

Color Gradients: Every fill ratio is painted in a different color gradient that corresponds to the levels of resistance. Red: FR 15%, Blue: FR 25%, Green: FR 50%, Purple: FR 85%.

Figure 19. The condenser resistance cloud map of the fill ratios of 15%, 25%, 50%, and 85%

5.6 Comparisons with other works

The numerical data that has been given in the literature for wickless heat pipe and which can be compared with the present experimental values are the curve of evaporator wall temperature. Figure 20 presents the comparison between the present numerical findings and the findings of Andrzejczyk [25]. From this, it is evident that both the evaporator wall temperatures have the same pattern but with a variation of 12% in the range of input power of 10 to 100 W.

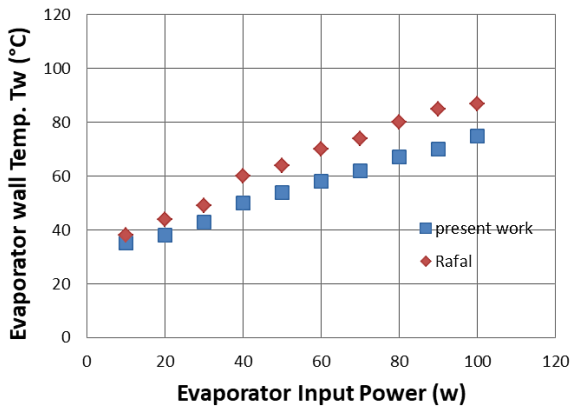

Figure 20. Comparison between the present experimental results and results [25]

6. CONCLUSIONS

This research is important because it aims to deepen the knowledge of the main parameters that affect the thermal characteristics of evaporative cooling systems. The novelties introduced in the heat transfer enhancement research of this work, namely, temperature and resistance cloud maps, can be used as effective tools by engineers and researchers to visualize and analyze the thermal performance and enhance it. In summary, this work contributes to the state of knowledge in thermal management and provides useful recommendations for enhancing the performance of evaporative cooling systems.

Key innovations and contributions of this study include:

1. Detailed Analysis of Fill Ratios

- This research work shall also give a clear insight on how the various fill ratios (15%, 25%, 50% and 85%) affects the theoretical wall evaporator temperature.
- The work also shows the conditions in which both liquid and vapor phases are filled to the required proportions, hence the efficiency of heat transfer and temperature control.

2. Thermal Performance Mapping

- The research also presents temperature cloud maps and condenser resistance cloud maps with different fill ratios, which is a new way to express thermal performance under various operating conditions.
- These maps help in the analysis of temperature distribution and the effectiveness of heat transfer with an aim of enhancing the design of evaporative cooling systems.

3. Impact of Flow Rate for Cooling Water

- Although actual figures of the cooling water flow rates were not given, the study deduces general principles to advance the importance of the aspect in enhancing thermal performance.
- Turning to the discussion, it is possible to mention the necessity of the cooling water flow rates' management to increase the heat transfer rate and energy utilization efficiency.

4. Comprehensive Data Analysis

- First, the systematic approach of the research is presented in terms of the variation of theoretical wall evaporator temperature and condenser resistance as a function of evaporator input power.
- Thus, the findings suggest fill ratios and cooling water flow rates should be well chosen to enable the expected thermal performance to be delivered.

5. Practical Implications

- They provide useful guidelines on how to design and run evaporative cooling systems, the fill ratio and the effectiveness of the cooling process together with the energy used in the process.
- The study offers a platform for increased research and development concerning the adopted cooling strategies in several applications.

The research identifies the following directions for further investigations to enhance the knowledge of and enhance evaporative cooling systems. They are experimental verification, controlling the flow rates of cooling water, dynamic performance, new heat transfer, photovoltaic integration, material and configuration investigation, environmental impacts, economic and ecological assessment, optimization techniques, and real-time intelligent control. These areas are to overcome the existing shortcomings and broaden the scope of knowledge and practical application of evaporative cooling systems for the creation of improved, dependable, and efficient cooling systems. The research also seeks to establish the effects of environmental factors on the evaporative cooling systems to come up with better and more sustainable designs.

ACKNOWLEDGMENT

The authors would like to express their thanks to Mustansiriyah University (www. uomustansiriyah.edu.iq) In Baghdad – Iraq for its support in the present study.

REFERENCES

[1] Webb, R.L. (2002). Test results on a thermosyphon concept to high-power cool desktop computers and servers. In Eighteenth Annual IEEE Semiconductor Thermal Measurement and Management Symposium. Proceedings 2002 (Cat.No.02CH37311), San Jose, CA, USA, pp. 151-158. https://doi.org/10.1109/STHERM.2002.991361

[2] Vasiliev, L.L. (2005). Heat pipe in modern heat exchangers. Applied Thermal Engineering, 25(1): 1-19. https://doi.org/10.1016/j.applthermaleng.2003.12.004

[3] Japiksey, D. (1973). Advances in thermosyphon technology. Advances in Heat Transfer, 99: 1-111. https://doi.org/10.1016/S0065-2717(08)70061-3

[4] Al Jubori, A.M., Jawad, Q.A. (2020). Computational evaluation of thermal behavior of a wickless heat pipe under various conditions. Case Studies in Thermal Engineering, 22: 100767. https://doi.org/10.1016/j.csite.2020.100767

[5] Barrak, A.S., Saleh, A.A.M., Naji, Z.H. (2020). Experimental and numerical simulation for thermal investigation of oscillating heat pipe using VOF model. Engineering and Technology Journal, 38(1): 88-104. https://doi.org/ 10.30684/etj.v38i1A.286

[6] Kim, Y., Shin, D.H., Kim, J.S., You, S.M., Lee, J. (2019). Effect of sintered microporous coating at the evaporator on the thermal performance of a two-phase closed thermosyphon. International Journal of Heat and Mass Transfer, 131: 1064-1074. https://doi.org/10.1016/j.ijheatmasstransfer.2018.11.134

[7] Wang, X., Wang, Y., Chen, H., Zhu, Y. (2018). A combined CFD/visualization investigation of heat transfer behaviors during geyser boiling in two-phase closed thermosyphon. International Journal of Heat and Mass Transfer, 121: 703-714. https://doi.org/10.1016/j.ijheatmasstransfer.2018.01.005

[8] Eidan, A.A., Najim, S.E., Jalil, J.M. (2016). Experimental and numerical investigation of thermosyphone performance in HVAC system applications. Heat and Mass Transfer, 52: 2879-2893. https://doi.org/10.1007/s00231-016-1800-y

[9] Alamnar, A.A., Al-Dadah, R.K., Mahmoud, S.M. (2016). Numerical investigation of effect of fill ratio and inclination angle on a thermosiphon heat pipe thermal performance. Applied Thermal Engineering, 108: 1055-1065. https://doi.org/10.1016/j.applthermaleng.2016.07.163

[10] Fadhl, B., Wrobel, L.C., Jouhara, H. (2015). CFD model of two-phase due thermosyphon charged with R134a and R404a. Applied Thermal Engineering, 78: 482-490. https://doi.org/10.1016/j.applthermaleng.2014.12.062

[11] Abdullahi, B. (2015). Development and optimization of heat pipe based compound parabolic collector. Thesis submitted to University of Birmingham.
[12] Anjankar, P.G., Yarasu, R. (2012). Experimental analysis of condenser length effect on the performance of thermosyphon. International Journal of Emerging Technology and Advanced Engineering, 2(3): 494-499.
[13] Jiao, B., Qiu, L.M., Zhang, X.B., Zhang, Y. (2008). Investigation on the effect of filling ratio on the steady-state heat transfer performance of a vertical two-phase closed thermosiphon. Applied Thermal Engineering, 28(11-12): 1417-1426. https://doi.org/10.1016/j.applthermaleng.2007.09.009
[14] Wang, Z., Turan, A., Craft, T. (2023). Numerical investigation of the two-phase closed thermosyphon operating with non-uniform heat flux profiles. Energies, 16(13): 5141. https://doi.org/10.3390/en16135141
[15] Alkhafaj, O.R., Yasin, N.J., Al-abbas, A.H. (2023). Optimization of wickless heat pipe heat exchanger using R1234-yf and ethanol as working fluids. International Journal of Applied Science and Engineering, 20(3): 2023124. https://doi.org/10.6703/IJASE.202309_20(3).004
[16] Cary, V.P. (1992). Liquid Vapor Phase Change Phenomena: An Introduction to the Thermophysics of Vaporization and Condensation Processes in Heat Transfer Equipment, Second Edition. CRC Press.
[17] Holman, J.P. (1997). Heat Transfer. 8th ed. McGraw-Hill Kogakusha.
[18] Joud, K.A., Al-Tabbakh, A.A. (2015). A theoretical procedure for estimating saturation temperature inside solar two-phase loops. Journal of Engineering and Sustainable Development, 19(4): 219-248.
[19] Price, H.W., Klein, S.A., Beckman, W.A (1986). Analysis of boiling plate collectors. Journal of Solar Energy Engineering, 108(2): 150-157. https://doi.org/10.1115/1.3268083
[20] Incorporeal, F.P., Dewitt, D.P. (1999). Fundamentals of Heat and Mass Transfer. 3d ed., Johan Wiley and Sons.
[21] El-Assy, A.Y., Clark, J.A (1988). Thermal analysis of a flat-plate collector in multiphase flows, including superheat. Solar Energy, 40(4): 345-361. https://doi.org/10.1016/0038-092X(88)90007-2
[22] Roshenow, W.M (1952). A method of correlating heat transfer data for surface boiling liquids. Journal of Fluids Engineering, 74(6): 969-976. https://doi.org/10.1115/1.4015984
[23] Incropera, F.P., DeWitt, D.P. (1996). Fundamentals of Heat and Mass Transfer (4th ed.). John Wiley & Sons.
[24] Peterson, G.P. (1994). An Introduction to Heat Pipes: Modeling, Testing, and Applications. Wiley-Interscience.
[25] Andrzejczyk, R. (2018). Experimental investigation of the thermal performance of a wickless heat pipe operating with different fluids: water, ethanol and SES36. Analysis of influences of instability processes at working operation parameters. Energies, 12(1): 1-28.

NOMENCLATURE

A	Area
c_p	Specific heat at constant pressure
D	Diameter of pipe
H	Head of working fluid
h	Heat transfer coefficient
h_{fg}	Latent heat of vaporization
K	Thermal conductivity
L	Length
$\dot{m}$	Mass flow rate
$\dot{m}_w$	Cooling water mass flow rate
P	Pressure
q_2	Boiling heat flux
Q_{heater}	Heat input of heater
Q_w	Useful heat gain to the water jacket
I	Times current
R	Resistance
R_e	Reynolds Number $= \frac{\rho \vartheta D}{\mu}$
T_a	Ambient temperature
T_{cw}	Average water jacket temperature
T_{sat}	Saturation temperature
T_w	Evaporator wall temperature
T_{w1}	Water cooling inlet temperature
T_{w1}	Water cooling outlet temperature
V	Voltage